Inorg. Chem. **2006**, *45*, 1774–1782

Magneto-Structural Correlations in $Cu(tn)Cl_2$ (tn = 1,3-Diaminopropane): Two-Dimensional Spatially Anisotropic Triangular Magnet Formed by Hydrogen Bonds

Vladimír Zeleňák,*,† Alžbeta Orendáčová,‡ Ivana Císařová,§ Juraj Černák,† Oxana V. Kravchyna,‖ Ju-Hyun Park,⊥ Martin Orendáč,‡ Alexander G. Anders,‖ Alexander Feher,‡ and Mark W. Meisel⊥

Institute of Chemistry, Department of Inorganic Chemistry, Faculty of Science, P. J. Šafárik University, Moyzesova 11, 041 54 Košice, Slovak Republic, Institute of Physics, Centre of Low-Temperature Physics of Slovak Academy of Sciences and P. J. Šafárik University, Park Angelinum 9, 041 54 Košice, Slovak Republic, Department of Inorganic Chemistry, Faculty of Science, Charles University, Hlavova 2030, Prague, Czech Republic, Institute for Low-Temperature Physics and Engineering, Lenin Avenue 47, 310164 Kharkov, Ukraine, and Department of Physics and Center for Condensed Matter Sciences, University of Florida, Gainesville, Florida 32611-8440

Received September 20, 2005

A novel polymeric one-dimensional compound $Cu(tn)Cl_2$ (tn = 1,3-diaminopropane) was prepared and structurally characterized, and its spectral, magnetic, thermodynamic, and thermal properties were studied. The unique structure shows ladderlike chains composed of Cu^{II} atoms and chloro bridging ligands [$Cu(-\mu_3\text{-}Cl-)Cu_2$] running along the crystallographic *c* axis. The coordination geometry about copper (4 + 2) approximates that of a strongly elongated octahedron. The equatorial plane of the coordination octahedron is formed by a chelate N-bonded tn ligand and two chloro ligands. One of the chloro ligands is terminal, and the other one, μ_3-Cl^-, forms two additional longer bonds to the neighboring copper atoms and thus occupies the axial octahedral positions. The electronic ground state of the Cu^{II} ion is of d_{z^2} symmetry and suggests the activation of intraladder and interladder Cl···H–N hydrogen bonds as exchange paths that form a two-dimensional pattern of a triangular symmetry. The interaction due to the hydrogen bonds seems to play an important role in molecular packing and magnetic coupling. The studies of magneto-structural correlations including electron paramagnetic resonance measurements and thermodynamic and magnetic properties revealed a two-dimensional character of magnetic correlations with the effective intralayer exchange coupling $J/k_B \approx -3$ K. No phase transition to the ordered state has been observed down to 60 mK. $Cu(tn)Cl_2$ with the interlayer coupling $J' \approx 10^{-3}J$ and moderate intralayer interaction represents an excellent example of a two-dimensional magnetic system.

Introduction

The magnetic properties of solids are a presently intensively studied area of chemistry and physics. A significant amount of attention has been devoted to the synthesis of the compounds of tunable dimensionality because the resulting solids have potential applications as molecular-based magnetic materials.[1] In the last few decades, low-dimensional magnetic systems have attracted special interest stimulated by the physics of exotic superconductors in which the magnetic subsystem plays an important role in the formation of Cooper pairs.[2]

In our work, we are interested in the study of the polymeric chainlike materials, especially those with alternating bridging

* To whom correspondence should be addressed. E-mail: zelenak@upjs.sk.
† Institute of Chemistry, Department of Inorganic Chemistry, Faculty of Science, P. J. Šafárik University.
‡ Institute of Physics, Centre of Low-Temperature Physics of Slovak Academy of Sciences and P. J. Šafárik University.
§ Charles University.
‖ Institute for Low-Temperature Physics and Engineering.
⊥ University of Florida.

(1) (a) Gatteschi, D.; Kahn, O.; Miller, J. S.; Palacio, F. *Magnetic Molecular Materials;* Kluwer Academic Publishers: Dordrecht, The Netherlands, 1991. (b) Kahn, O. *Molecular Magnetism*; VCH Publishers: Weinheim, Germany, 1993. (c) Miller, J. S. *Inorg. Chem.* **2000**, *39*, 4392.
(2) (a) Dagotto, E. *Phys. World* **1996**, *9*, Apr 22. (b) Tranquada, J. M.; Ichikawa, N.; Uchida, S. *Phys. Rev.* **1999**, *B59*, 14712.

10.1021/ic0516109 CCC: $33.50
Published on Web 01/17/2006

groups, because they are suitable model compounds for the investigation of magnetic chains with alternating nearest-neighbor exchange coupling.[3] From the structural point of view, these one-dimensional (1D) systems contain paramagnetic centers (metal ions) linked by suitable ligands (cyano, halogeno, azido, etc.), forming linear or bent chains, ladders, or ribbons.[4] The synthesis and design of the polynuclear complexes with the interesting magnetic properties can be achieved also by self-assembly of the metal carboxylates and the chelating organic ligands.[5] During the preparation of alternating chain structures containing dinuclear copper acetato groups, we have unexpectedly obtained Cu(tn)Cl$_2$ (tn = 1,3-diaminopropane), a 1D polymer formed by ladderlike infinite chains with μ_3-bridging chloro ligands. Although the crystal structure of Cu(tn)Cl$_2$ is relatively simple, its structure type is rather unique.[6,7] The investigation of magneto-structural correlations presented in this work revealed the important role of the hydrogen bonds in the formation of a two-dimensional (2D) spatially anisotropic triangular lattice. The excellent low dimensionality and moderate values of physical parameters predetermine the compound as a good model system for the study of low-dimensional magnetic properties in the broad range of temperatures and magnetic fields.

Herein, we report the synthesis, crystal structure, and magnetic, thermodynamic, and spectral properties of the compound Cu(tn)Cl$_2$ (further denoted as CTCL), a ladderlike 1D polymer.

Experimental Section

Preparation of CTCL. First, the compound Cu(CH$_3$COO)$_2$(tn)$_2$ was prepared according to the modified procedure.[8] Starting with 1 g (5 mmol) of copper acetate dissolved in 50 cm^3 of a water/ethanol mixture (1:1, v/v), 0.85 cm^3 (10 mmol) of tn was added. The violet solution was filtered and set aside. After several days at room temperature, a blue-violet solid of Cu(CH$_3$COO)$_2$(tn)$_2$ crystallized, which was then filtered off and dried. The solid was sensitive to humidity and therefore was kept in a desiccator over silica gel.

The complex CTCL was prepared by diffusion of carbon tetrachloride (CCl_4) to the methanol solution of Cu(CH$_3$COO)$_2$(tn)$_2$ (3 mmol in 40 cm^3 of CH$_3$OH). After 2 days, blue-green crystals were formed and separated by filtration. Unlike Cu(CH$_3$COO)$_2$(tn)$_2$, the obtained product is stable in air at room temperature. Anal. Calcd for $C_3H_{10}N_2Cl_2Cu$: C, 17.27; H, 4.83; N, 13.43. Found: C, 17.47; H, 4.57; N, 12.78. IR (KBr disk): 3276s, 3227s, 3124w, 2957w, 2945w, 2920m, 2874m, 1572vs, 1463w, 1453w, 1440w, 1396vw, 1321vw, 1276m, 1165vs, 1148s, 1104s, 1074s, 1028s, 930s, 879m, 664s, 618w, 502m, 417w cm^{-1}. UV−vis ($BaSO_4$ as the reference material): 39 000, 34 900, 30 600sh, 14 700 cm^{-1}.

Physical Measurements. The infrared (IR) spectrum was recorded with an Avatar 330 (Nicolet) Fourier transform (FT-IR) spectrophotometer using a KBr disk. The electronic spectra were obtained with a Specord M-40 UV−vis spectrophotometer using a solid-state sample with $BaSO_4$ as the reference material. Thermogravimetric (TG) and differential thermal analytic (DTA) measurements were performed in the presence of air flow (50 cm^3/min) while heating at the rate of 6 °C/min by means of a NETZSCH STA 409 apparatus. The X-ray diffraction (XRD) patterns were recorded with a Micrometa diffractometer using Cr Kα, V-filtered radiation. The elemental analysis was performed with a Perkin-Elmer 2400 CHN elemental analyzer. The susceptibility and magnetization were studied using a commercial SQUID magnetometer. A powdered specimen of 168 mg was fixed in a standard gelatin capsule that was held by a plastic straw. The magnetic data were corrected for the diamagnetic contribution of the sample holder. The specific heat measurements were performed in the temperature range from 60 mK to 6.5 K using a dual-slope method[9] in an Oxford Instruments dilution refrigerator. A powdered sample was compressed to a thin coin-shaped pellet, of 34 mg, which was used for the specific heat measurements. The contribution of a calorimeter was subtracted from the total heat capacity. The electron paramagnetic resonance (EPR) experiment was performed with a homemade probe and spectrometer operating at 72.8 GHz, in the temperature region from 4 to 20 K. The EPR spectra were recorded on the powdered sample in the cylindrical cavity resonator operating in TE_{013} mode. The values of the magnetic field were calibrated by the *g*-marker 1,1′-diphenyl-2-picrylhydrazyl (DPPH).

X-ray Crystallography. The complex crystallized as air-stable, blue-green needles. The diffraction experiments were performed with a Nonius Kappa CCD diffractometer (Mo Kα radiation, λ = 0.710 70 Å) equipped with a graphite monochromator and a low-temperature apparatus. The details of data collection and refinement are summarized in Table 1. The data were corrected for Lorentz and polarization factors. An absorption correction based on the symmetry-related measurements was applied.[10a] The structure was solved in a noncentrosymmetric space group $Pna2_1$ by the heavy-atom method using the *SHELXS-86* program.[10b] The structure was refined on F^2 using the *SHELXL-97* program[10c] as a racemic twin [the Flack parameter was 0.47(4)]. During the refinement, the electron density distribution around the carbon atoms of the chelate ring indicated the presence of strong disorder (or dynamic motion of the carbon atoms). Several models as well as one in the centrosymmetric space group *Pnma* describing the observed situation were tried, and finally the best results were obtained from the model considering (i) the presence of two disordered positions for every carbon atom, (ii) the restraints of the C−N and C−C bond distances, respectively, to be the same in both disordered positions, and (iii) an isotropic thermal motion of the carbon atoms. The occupancy factors of both disordered positions were refined to the final values 0.63(3) and 0.37(3), respectively. Hydrogen atoms

(3) Garrett, A. W.; Nagler, S. E.; Tennant, D. A.; Sales, B. C.; Barnes, T. *Phys. Rev. Lett.* **1997**, *79*, 745.
(4) (a) Černák, J.; Orendáč, M.; Potočňák, I.; Chomič, J.; Orendáčová, A.; Skoršepa, J.; Feher, A. *Coord. Chem. Rev.* **2002**, *224*, 51. (b) Abu-Youssef, M. A. M.; Escuer, A.; Goher, M. A. S.; Mautner, F. A.; Reiss, J. G.; Vicente, R. *Angew. Chem.* **2000**, *112*, 1681. (c) Gao, E. Q.; Bai, S. Q.; Wang, C. F.; Yue, Y. F.; Yan, C. H. *Inorg. Chem.* **2003**, *42*, 8456.
(5) (a) Mukherjee, P. S.; Maji, T. K.; Mostafa, G.; Ribas, J.; El-Fallah, M. S.; Chaudhuri, N. R. *Inorg. Chem.* **2001**, *40*, 928. (b) Miller, J. S.; Epstein, J. *Angew. Chem., Int. Ed. Engl.* **1994**, *33*, 385. (c) Rochon, F. D.; Melanson, R.; Andruh, M. *Polyhedron* **1996**, *151*, 3075. (d) Meenakumari, S.; Tiwari, S. K.; Chakravarty, A. R. *J. Chem. Soc., Dalton Trans.* **1993**, 2175.
(6) Harvey, D.; Lock, C. J. L. *Acta Crystallogr.* **1986**, *C42*, 799.
(7) Andreetti, G. D.; Cavalca, L.; Pellinghelli, M. A.; Sgarabotto, P. *Gazz. Chim. Ital.* **1971**, *101*, 488.
(8) (a) Melník, M.; Nasanen, R. *Suomen Kemistilehti* **1970**, *B43*, 99. (b) Melník, M.; Taiminen, A. M. *Suomen Kemistilehti* **1971**, *B44*, 8.
(9) Riegel, S.; Weber, G. *J. Phys.* **1986**, *E19*, 790.
(10) (a) Blessing, R. H. *J. Appl. Crystallogr.* **1997**, *30*, 421. (b) Sheldrick, G. M. *Acta Crystallogr.* **1990**, *46*, 467. (c) Sheldrick, G. M. *SHELXL-97, Program for the Refinement of Crystal Structures*; University of Göttingen: Göttingen, Germany, 1997. (d) Brandenburg, K. *DIAMOND*, version 2.1e; Crystal Impact GbR: Bonn, Germany, 2000. (e) Nardelli, M. J. *Appl. Crystallogr.* **1995**, *28*, 659.

Table 1. Crystal Data and Structure Refinement of CTCL

empirical formula	$CuCl_2C_3H_{10}N_2$
formula weight	208.57
Crystal Parameters	
crystal shape	needles
crystal color	blue green
crystal size (mm)	0.45 × 0.1 × 0.05
crystal system	orthorhombic
space group	$Pna2_1$ (No. 33)
unit cell dimensions	
a (Å)	17.9560(1)
b (Å)	6.8590(2)
c (Å)	5.7100(5)
V_c (Å^3)	706.94(7)
molecules per cell, Z	4
D_x (g/cm^3)	1.960
Measurement of the Intensity Data	
instrument	Nonius Kappa CCD
temperature (K)	150(2)
radiation λ (Å)	0.710 70
monochromator	graphite
scan mode	φ and ω
θ range (deg)	3.16−27.47
reflns measd	11129
independent reflns	1478
reflns obsd	1372 ($I \geq 2\sigma(I)$)
linear abs coeff, μ (mm^{-1})	3.743
F(000)	420
reflns for cell measurement	6417 with $1 \leq \theta \leq 27.5$
index limits	
h	−23 to +23
k	−8 to +8
l	−6 to +7
Refinement	
refinement method	full-matrix least squares on F^2
parameters	72
Flack parameter	0.47(4)
GOF on F^2	1.033 (obsd), 1.035 (all)
R1	0.0267 (obsd), 0.0293 (all)
wR2	0.0690 (obsd), 0.0706 (all)
max/min height in the final difference synthesis (e/Å^3)	0.369/−0.489

were placed in their calculated positions using isotropic thermal parameters tied to the parent atoms ($1.2U_{eq}$). The final reliability values are summarized in Table 1. All structure drawings were generated using *DIAMOND* software.[10d] Selected bond distances and angles are listed in Table 2. The hydrogen bonds and the nonbonding contacts were calculated using PARST.[10e]

Results and Discussion

Synthesis. The synthesis of the polynuclear complexes with interesting magnetic properties can be achieved by self-assembly of the metal carboxylates with the chelating organic ligands.[5] We have used acetato and tn ligands, which may both possess bridging roles.[11] By the modified procedure,[8] we have prepared the compound $Cu(CH_3COO)_2(tn)_2$, hygroscopic crystals of poor quality. Our attempt to recrystallize them unexpectedly yielded the title compound CTCL. However, the aforementioned synthetic procedure is reproducible. CCl_4 can be considered as the source of the chloro ligands. It was shown that metal halide or oxide based

Table 2. Selected Bond Distances (Å) and Angles (deg) in CTCL[a]

Bond Distances			
Cu−Cl1	2.3098(6)	N1−C1′	1.51(1)
Cu−Cl2	2.3281(6)	N2−C3	1.470(6)
Cu−N1	2.014(2)	N2−C3′	1.47(1)
Cu−N2	2.006(2)	C1−C2	1.502(9)
Cu−Cl2^{i}	2.873(3)	C2−C3	1.543(9)
Cu−Cl2^{ii}	2.864(3)	C1′−C2′	1.51(1)
N1−C1	1.468(8)	C2′−C3′	1.50(1)
Bond Angles			
N2−Cu−N1	95.80(9)	N2−C3−C2	112.4(7)
N2−Cu−Cl1	88.85(7)	N1−C1′−C2′	115(1)
N1−Cu−Cl1	175.31(7)	C3′−C2′−C1′	105(1)
N2−Cu−Cl2	177.5(2)	N2−C3′−C2′	116(1)
N1−Cu−Cl2	85.05(6)	Cl1−Cu−Cl2^{ii}	94.49(6)
Cl1−Cu−Cl2	90.29(2)	Cl1−Cu−Cl2^{i}	94.28(6)
C1−N1−Cu	122.4(5)	N1−Cu−Cl2^{ii}	85.3(3)
C1′−N1−Cu	120.9(6)	N1− Cu−Cl2^{i}	86.5(3)
C3−N2−Cu	124.2(3)	N2−Cu−Cl2^{ii}	84.3(2)
C3′−N2−Cu	120.0(7)	N2−Cu−Cl2^{i}	89.3(2)
N1−C1−C2	110.1(8)	Cl2−Cu−Cl2^{ii}	93.42(8)
C1−C2−C3	117.6(9)	Cl2−Cu−Cl2^{i}	93.19(7)
		Cl2^{i}-Cu−Cl2^{ii}	168.98(3)

[a] Symmetry codes: (i) $-x$, $1-y$, $0.5+z$; (ii) $-x$, $1-y$, $-0.5+z$.

catalysts decompose CCl_4, yielding chloride ions as one of the products of the decomposition.[12]

Our attempts to prepare the title compound directly from the reaction of copper chloride and tn in an aqueous solution were unsuccessful because this type of complex is difficult to prepare without using a coordinated solvent. In their attempt to synthesize the simple 1,3-diaminopropane compound $Cu(tn)_2Cl_2$, Sundberg et al. prepared two binuclear solvates, namely, aquabis(1,3-diaminopropane)copper(II) dichloride, $[Cu(H_2O)(tn)_2]Cl_2$, and chlorobis(1,3-diaminopropane)copper(II) chloride methanol solvate, $[CuCl(tn)_2]Cl\cdot MeOH$.[13]

Description of the Structure. Views of the structure of CTCL are shown in Figures 1 and 2. One 1,3-diaminopropane molecule is present in the formula unit of CTCL. Complexes containing a $[Cu(tn)]^{2+}$ building block are scarce,[14] and more frequently a bis-chelate cation, $[Cu(tn)_2]^{2+}$, is formed.[13,15]

(11) (a) Ye, B. H.; Ji, L. N.; Xue, F.; Mak, T. C. W. *Polyhedron* **1998**, *17*, 2687. (b) Ackermann, H.; Weller, F.; Neumueller, B.; Dehnicke, K. *Z. Anorg. Allg. Chem.* **1999**, *625*, 147. (c) Bazzicalupi, C.; Bencini, A.; Bianchi, A.; Fusi, V.; Paoletti, P.; Valtancoli, B. *Inorg. Chim. Acta* **1996**, *244*, 255. (d) Sivý, P.; Valach, F.; Koreň, B.; Macášková, L.; Pavelčík, F.; Sivý, J. *Acta Crystallogr.* **1989**, *C45*, 1689.

(12) (a) Petrosius, S. C.; Drago, R. S.; Young, V.; Grunewald, G. C. *J. Am. Chem. Soc.* **1993**, *115*, 6131. (b) Khaleel, A.; Dellinger, B. *Environ. Sci. Technol.* **2002**, *36*, 1620. (c) Koper, O. B.; Wovchko, E. A.; Glass, J. A.; Yates, J. T.; Klabunde, K. J. *Langmuir* **1995**, *11*, 2054. (d) Smirnov, V. V.; Tarkhanova, I. G.; Kokorin, A. I.; Pergushov, V. I.; Tsvetkov, D. S. *Kinet. Catal.* **2005**, *46*, 65.

(13) Sundberg, M. R.; Sillanpaa, R.; Uggla, R. *Inorg. Chim. Acta* **1996**, *245*, 35.

(14) (a) Triki, S.; Thetiot, F.; Vandevelde, F.; Sala-Pala, J.; Gomez-Garcia, C. J. *Inorg. Chem.* **2005**, *44*, 4086. (b) Ribas, J.; Garcia, A.; Costa, R.; Monfort, M.; Alvarez, S.; Zanchini, C.; Solans, X.; Domenech, M. V. *Inorg. Chem.* **1991**, *30*, 841. (c) Hay, R. W.; Danby, A.; Lightfoot, P. *Polyhedron* **1997**, *16*, 3261. (d) Navarro, J. A. R.; Romero, M. A.; Salas, J. M.; Molina, J.; Tiekink, E. R. T. *Inorg. Chim. Acta* **1998**, *274*, 53. (e) Luo, J.; Zhou, X. G.; Weng, L. M.; Hou, X. F. *Acta Crystallogr.* **2003**, *C59*, 519. (f) Thetiot, F.; Triki, S.; Sala Pala, J.; Golhen, S. *Inorg. Chim. Acta* **2003**, *350*, 314.

(15) (a) Sundberg, M. R.; Kivekas, R.; Huovilainen, P.; Uggla, R. *Inorg. Chim. Acta* **2001**, *324*, 212. (b) Sundberg, M. R.; Uggla, R. *Inorg. Chim. Acta* **1997**, *254*, 259. (c) Sundberg, M. R.; Tylli, H.; Matikainen, J.; Book, T.; Uggla, R.; Valkeapaa, M. *Inorg. Chim. Acta* **1997**, *266*, 47. (d) Sundberg, M. R.; Sillanpaa, R.; Jokela, J. *Inorg. Chim. Acta* **1996**, *248*, 1. (e) Sundberg, M. R.; Koskimies, J. K.; Matikainen, J.; Tylli, H. *Inorg. Chim. Acta* **1998**, *268*, 21. (f) Sillaupti, R.; Jokela, J.; Sundberg, M. R. *Inorg. Chim. Acta* **1997**, *258*, 221.

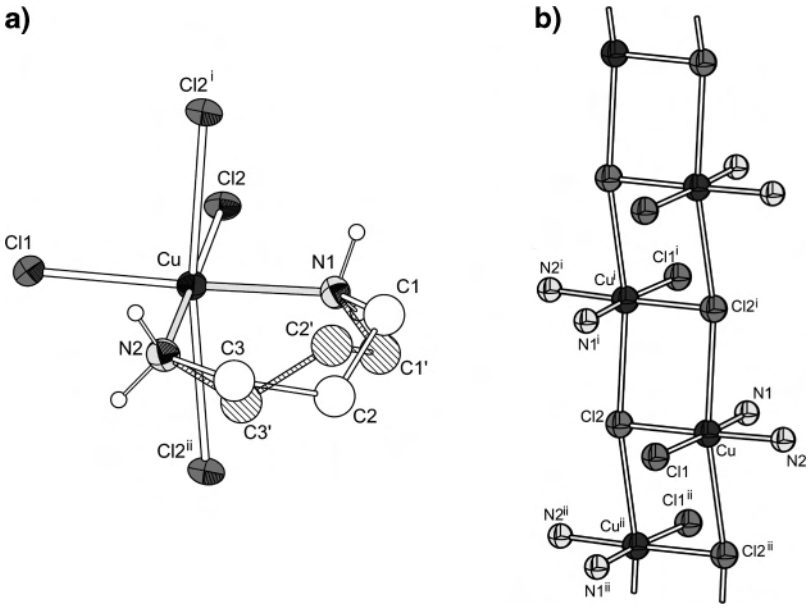

Figure 1. (a) Drawing of the CTCL molecule with an atom-labeling scheme. The thermal ellipsoids are drawn at the 50% probability level. Hydrogen atoms bonded to carbon atoms are omitted for the sake of clarity. The less populated positions of the atoms in the chelate ring are drawn by dashed lines. (b) View of the 3,3-ladderlike structure of CTCL running along the crystallographic *c* axis. Carbon and hydrogen atoms are omitted for the sake of clarity. Symmetry codes: (i) $-x, 1-y, 0.5+z$; (ii) $-x, 1-y, -0.5+z$.

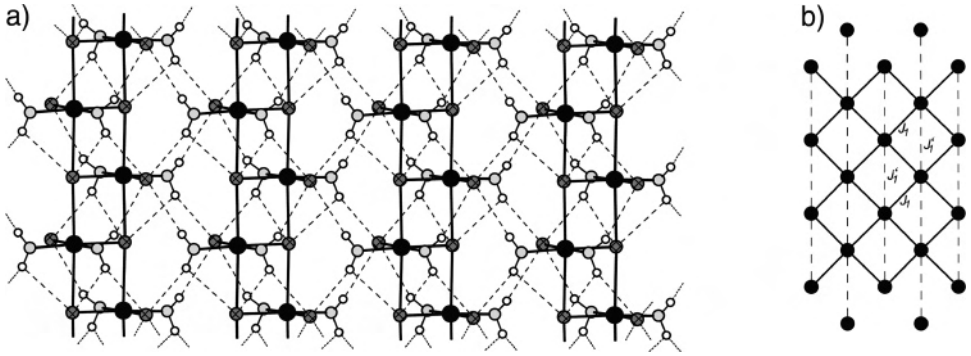

Figure 2. (a) View of the intermolecular hydrogen-bond system in CTCL approximately along the *a* axis (dashed lines): black, copper atoms; gray, nitrogen atoms; hatched, chlorine atoms; white, hydrogen atoms. Carbon atoms are omitted for the sake of clarity. Only the more populated positions of hydrogen atoms bonded to N atoms are shown. (b) Schematic drawing of the triangular magnetic lattice with exchange couplings of J_1 and J_1'.

The copper atom is coordinated in the 4 + 2 form because of the presence of the Jahn−Teller effect. The chelate tn ligand (bonded through the nitrogen atoms) and two chloro ligands are coordinated in the equatorial plane. One of the chloro ligands (Cl1) is terminal, and the second one (Cl2) is a μ_3-bridging ligand. The coordination sphere of the Cu^{II} in the axial positions is completed by two μ_3-chloro ligands from two adjacent CTCL units (two Cl2 with the following symmetry codes: $-x, 1-y, 0.5+z$ and $-x, 1-y, -0.5+z$, respectively). The $Cl2^{i}-Cu-Cl2^{ii}$ angle in the bridge is 168.9(4)°. From a structural point of view, this arrangement results in the formation of a 3,3-ladder system (for notation, see ref 4a) running along the crystallographic *c* axis (Figure 1b). A survey of the Cambridge Structural Database[16] gave only two citations of similar complexes, namely, Cu(en)Cl_2 (en = ethylenediamine) and Cd(tn)Cl_2.[6,7]

The observed Cu−Cl1 distance in the complex CTCL is somewhat shorter than Cu−Cl2 in the equatorial plane [2.3098(6) and 2.3281(6) Å, respectively]. This fact is in accordance with the bridging function of the Cl2 ligand. The mean axial Cu−Cl2 distance, 2.868 Å, is similar to that in the en analogue Cu(en)Cl_2 (2.887 Å).[6]

The geometric parameters are gathered in Table 2. The observed Cu−N bond lengths [2.006(2) and 2.014(2) Å, respectively] are similar to those found in the copper (1,3-diaminopropane)carboxylato complexes with octahedral coordination of the copper atom.[15] The bite angle of the chelated tn is 95.85(2)°. The widening from the ideal 90° value can be due to the hydrogen bonding (see below). Further discussion and comparison of the geometric parameters concerning the tn ligand would not be appropriate because of the observed disorder of the carbon atoms. It is known that the six-membered ring formed by the tn and metal ion possesses great conformational freedom (chair or boat form), with the chair conformation being energetically more stable.[13,15,17] Both disordered forms of the Cu-tn metallocycle in CTCL (see Figure 1) adopt this chairlike conformation.

(16) Allen, F. H. *Acta Crystallogr.* **2002**, *B58*, 380.

(17) Gollogly, J. R.; Hawkins, C. J. *Inorg. Chem.* **1972**, *11*, 156.

Table 3. Intermolecular Hydrogen Bonds in CTCL[a]

D−H···A	D−H [Å]	H···A [Å]	D···A [Å]	DHA [deg]
N1−H1···Cl1^{i}	0.900	2.666	3.506(8)	156
N1−H1···Cl2^{i}	0.900	2.904	3.365(8)	113
N1−H1′···Cl1^{i}	0.900	2.617	3.506(8)	169
N2−H10···Cl2^{i}	0.900	2.888	3.329(7)	112
N1−H2···Cl1^{ii}	0.900	2.693	3.544(7)	158
N1−H2′···Cl1^{ii}	0.900	2.665	3.544(7)	166
N2−H9···Cl1^{iii}	0.900	2.821	3.563(7)	140
N2−H9′···Cl1^{iii}	0.900	2.699	3.563(7)	161
N2−H10···Cl1^{iv}	0.900	2.579	3.413(7)	154
N2−H10′···Cl1^{iv}	0.900	2.647	3.413(7)	144

[a] Symmetry codes: (i) $-x, -y + 1, z - 0.5$; (ii) $-x, -y + 1, z + 0.5$; (iii) $-x, -y, z + 0.5$; (iv) $-x, -y, z - 0.5$.

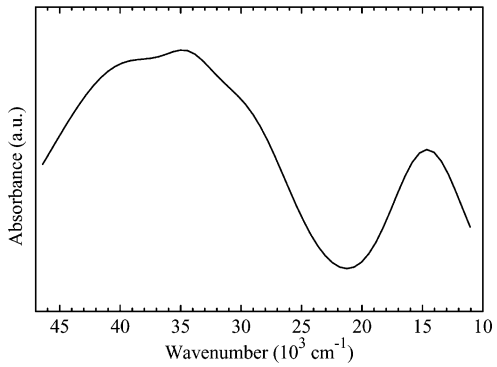

Figure 3. Diffuse-reflectance UV−vis spectrum of CTCL.

The adjacent 3,3 ladders in the *bc* plane are linked by intermolecular N−H···Cl hydrogen bonds (Figure 2 and Table 3) formed by all four hydrogen atoms (in both orientations) of the amino groups. Considering these hydrogen bonds, the structure can be viewed as a 2D hydrogen-bonded polymer. In the *a* direction, the formed layers are connected by very weak C−H···Cl type interactions with H···Cl distances of 2.90 Å (H5···Cl1) and 2.96 Å (H5′··· Cl1) in both orientations of the chelate ring.

Spectroscopic Studies. In the IR spectrum of the title compound, the absorption bands associated with the presence of the tn ligand were observed. The well-separated and narrow bands at 3276, 3227, and 3124 cm^{-1} can be assigned to $\nu(NH_2)$ stretching modes of tn. Their positions are, as is typical, shifted to lower wavenumbers because of the presence of N−H···Cl interactions.[18] Stretching vibrations of CH_2 groups of tn are at 2957, 2945, 2920, and 2874 cm^{-1}. The intensely sharp band at 1572 cm^{-1} is attributed to the deformation vibrations of CH_2 groups. The absorption band at 1165 cm^{-1} can originate from the ν(C−N) vibration. The other important absorption bands are summarized in the experimental part; these bands are mainly due to deformation vibrations and skeletal vibrations of CH_2 and NH_2 groups.[18]

The UV−vis spectrum of the complex CTCL is shown in Figure 3. The high-frequency region of the spectrum shows a broad absorption band as an envelope of three bands centered at 39 000, 34 900, and 30 600 cm^{-1}. These bands may be attributed to the amino-to-copper(II) and halogen-to-copper(II) ligand-to-metal charge-transfer (LMCT) transitions (σN → $d_{x^2-y^2}$ Cu^{II}; σ,πCl → $d_{x^2-y^2}$ Cu^{II}).[19a] Because six-coordinate tetragonal Cu^{II} complexes with long Cu−L bonds do not exhibit the CT absorption from the axially ligated halogeno ligands, we suppose that the halogen-to-copper transition is from the equatorial chloro ligands. In the visible region, the d−d transition from components of t_{2g} to the $d_{x^2-y^2}$ orbital was observed as a single peak centered at 14 700 cm^{-1}. No splitting of this band was observed. However, in the similar complex, Cu(en)Cl$_2$, three transitions were observed at 14 000, 15 000, and 13 000 cm^{-1}, respectively.[19b]

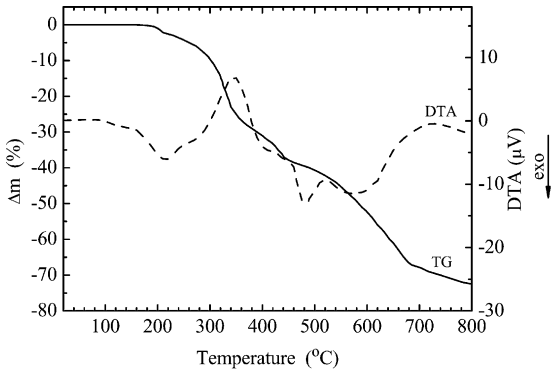

Figure 4. Thermoanalytical curves (TG/DTA) of the complex CTCL.

Thermal Studies. CTCL is stable up to 180 °C (see Figure 4). The first step of the decomposition, in the temperature range of 180−420 °C, can be attributed to the deamination, i.e., liberation of the organic portion of the molecule. The experimental weight loss of 37% is in agreement with the calculated value (tn) of 35.5%. As suggested by the DTA curve, this deamination process is complicated and appears on the DTA curve as an exothermic effect at 208 °C and an endothermic effect at 345 °C. The intermediates obtained by heating the sample to 250 and 370 °C were X-ray amorphous.

The weight loss, observed on the TG curve during heating above 420 °C, corresponds to the dehalogenation of the compound. The powder XRD analyses of the intermediates obtained by heating to 450 and 580 °C showed the peaks corresponding only to the CuCl phase (nantokite; PDF 6-0344). These results suggest that dehalogenation is an internal redox process. The further weight loss up to 800 °C can be attributed to the partial decomposition of CuCl. The final product was a mixture of CuCl (nantokite) and CuO (tenorite; PDF 45-0937) phases, as was confirmed by powder XRD.

Magnetic Study. The XRD studies performed at 150 K revealed strong tetragonal deformation of a local Cu^{II} coordination octahedron demonstrated by a large difference in the bond lengths; while Cu−Cl bond lengths in the apical positions are about 2.8 Å, the bonds Cu−Cl and Cu−N in the equatorial plane are much shorter, being equal to 2.3 and 2.0 Å, respectively. The observed strong elongation leads to the stabilization of the d_{z^2} electronic ground state of the Cu^{II} ion, and the unpaired electron should be described by a

(18) Bellamy, L. J. *The Infrared Spectra of Complex Molecules*; Chapman and Hall: London, 1975.

(19) (a) Lever, A. B. P. *Inorganic Electronic Spectroscopy*, 2nd ed.; Elsevier: Amsterdam, The Netherlands, 1984. (b) Hathaway, B. J.; Billing, D. E. *Coord. Chem. Rev.* **1970**, *5*, 143.

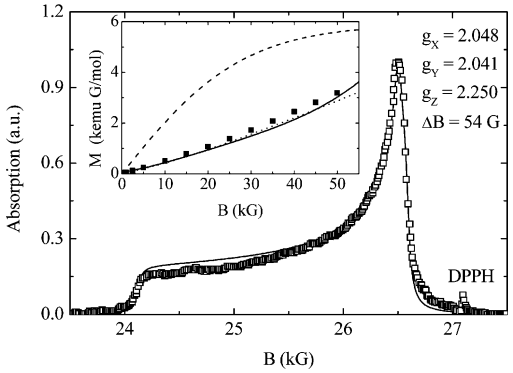

Figure 5. Magnetic field dependence of the EPR line shape of powdered CTCL at the temperature $T = 9.3$ K and the frequency 72.8 GHz. The solid line represents a theoretical prediction for a line shape of a polycrystalline sample with optimal g and ΔB parameters. Inset: Magnetic field dependence of the magnetization of powdered CTCL at the constant temperature $T = 2$ K. The dashed line corresponds to the free spin behavior described by the Brillouin function, and the solid and dotted lines represent theoretical predictions for the $S = {}^1/_2$ antiferromagnetic Heisenberg chain limit ($J_1 = 0$; $J_1'/k_B = -4.5$ K) and square lattice ($J_1/k_B = -3.0$ K; $J_1' = 0$), respectively. All calculations are performed for $g = 2.12$.

wave function of $d_{x^2-y^2}$ symmetry. Such an atomic arrangement prefers a potential formation of exchange pathways along the $d_{x^2-y^2}$ lobes within the equatorial plane. However, the given structure does not provide corresponding interatomic connections between Cu^{II} ions via covalent bonds (Figure 1b). A close inspection of the structure reveals a network of hydrogen bonds within and between the covalent ladders (Figure 2a), which can form exchange pathways, coupling the Cu^{II} spins in the *bc* plane into 2D magnetic layers of a triangular pattern with spatially anisotropic exchange coupling. The magnetic lattice can be treated as a square lattice with the nearest-neighbor interaction J_1 and one next-nearest-neighbor (diagonal) interaction J_1', which is equivalent to the spatially anisotropic triangular lattice and can be described by the J_1-J_1' model (see Figure 2b).[20] A weak spatial anisotropy in the nearest-neighbor interaction J_1 can be expected because of the slightly different geometrical parameters of intraladder and interladder hydrogen bonds. It should be noted that a mixing of d_{z^2} and $d_{x^2-y^2}$ states cannot be excluded; such a mixing could result in a partial activation of the exchange pathways through chloride atoms. Even in this case, there is no need to change the suggested magnetic model because the Cl bridges will form zigzag ladders, which represent segments of the supposed 2D triangular lattice.

The local symmetry of the Cu^{II} ion at helium temperatures has been studied by EPR measurements performed on a powdered sample in a temperature range from 4 to 20 K. The powder spectra are characterized by an asymmetric shape typical for a number of randomly oriented crystallites with the axial symmetry of a g tensor (Figure 5). The data were analyzed within a simple model including the effect of magnetic field, dipolar, and exchange coupling.[21] The model yields a theoretical prediction for the paramagnetic resonance line shape

$$I(B) = \int_{B_\parallel}^{B_\perp} \frac{(1 + B_\parallel^{-2}B'^2)}{[(B - B')^2\Delta B^2]B'^2(B_\perp^{\,2} - B'^2)^{1/2}} \qquad (1)$$

where $B_\parallel$, $B_\perp$, and ΔB represent the resonance parallel field, the perpendicular field, and the half-width at half-power, respectively. The analysis yielded the temperature dependence of the g factor and ΔB, as depicted in Figure 6. The observed Ising-like character of the g tensor, namely, $g_z > g_x, g_y$, reflects a strong tetragonal distortion of the local Cu^{II} octahedron. Consequently, the d_{z^2} electronic ground state of the Cu^{II} ion persists to lowest temperatures, and the aforementioned magnetic lattice model, suggested on the basis of the high-temperature structural data, can be applied to the analysis of magneto-structural correlations at helium temperatures. The observed temperature dependences of the g factor are rather weak and can be ascribed to a gradual deformation of the local octahedron with decreasing temperature. A weak in-plane g-factor anisotropy increasing below 20 K can be associated with the distortion of the local octahedron in the equatorial plane, as evidenced by X-ray studies at 150 K. Unlike the geometry of local Cu^{II} surroundings, the temperature dependence of the half-width is more significant. The observed divergent broadening of the EPR line at low temperatures is usually ascribed to the onset of the three-dimensional ordering.[22] The value of the critical temperature, T_c, has been estimated using the assumption about narrowing of the resonance line by the exchange coupling. The contribution of the dipolar coupling to the half-width, ΔB_{dip}, was evaluated using Van Vleck's moment method[23]

$$\Delta B_{dip} = M_2^{1/2} \qquad (2)$$

where M_2 is the second moment of the resonance line. The calculation for the CTCL structure yielded $M_2 = 1.903 \times 10^5$ G^2. The resulting estimate of the half-width, namely, $\Delta B_{dip} = 436$ G, is much higher than the largest experimental value (Figure 6), indicating the presence of the exchange coupling. The strength of the magnetic correlations was estimated within a mean-field approximation $B_{ex} = 9.063 \times 10^3$ G according to the relation derived in ref 24

$$\Delta B = M_2/B_{ex} \qquad (3)$$

using $\Delta B = 42$ G, the experimental value of the half-width of the resonance line taken at 20 K (Figure 6). This temperature should be sufficiently high to neglect the influence of a critical region. The critical temperature corresponding to the calculated exchange field, $g\mu_B B_{ex} = k_B T_c$, has been estimated as $T_c = 0.61$ K.

The magnetic susceptibility, χ, was measured in the temperature interval from 2 to 300 K in a field of 1 kG (Figure 7). It should be noted that the measurements performed during field cooling and zero field cooling yielded the same experimental results. The data were corrected for

(20) (a) Weinhong, Z.; McKenzie, R. H. *Phys. Rev.* **1999**, *B59*, 14367. (b) Manuel, L. O.; Ceccato, H. A. *Phys. Rev.* **1999**, *B60*, 9489.
(21) Ibers, J. A.; Swalen, J. D. *Phys. Rev.* **1962**, *127*, 1914.
(22) Kawasaki, K. *Prog. Theor. Phys.* **1968**, *39*, 285.
(23) Van Vleck, H. *Phys. Rev.* **1948**, *74*, 1168.
(24) Anderson, P. W.; Weiss, P. R. *Rev. Mod. Phys.* **1953**, *25*, 269.

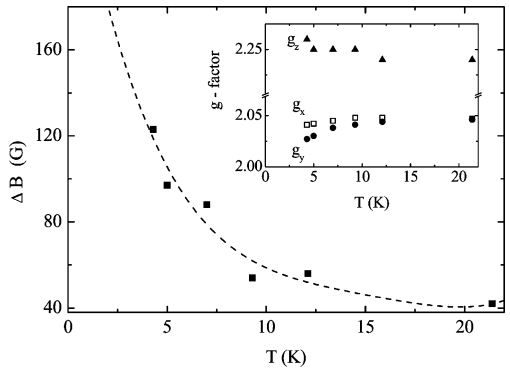

Figure 6. Temperature dependence of the half-width at half-power of the EPR resonance line. The dashed line is a guide for the eyes. Inset: Temperature dependence of the anisotropy of the g factor in CTCL.

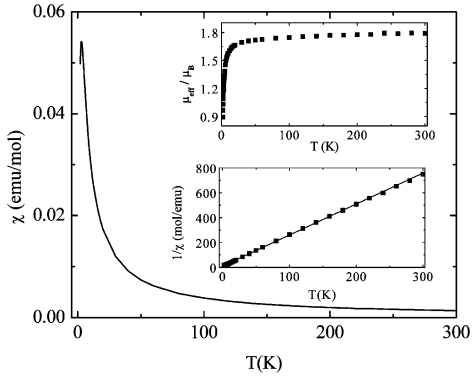

Figure 7. Temperature dependence of the magnetic susceptibility of powdered CTCL measured in the magnetic field of 1 kG. Upper inset: Temperature dependence of the effective magnetic moment of CTCL. Lower inset: Temperature dependence of the inverse susceptibility of CTCL. The solid line represents the results of a fit by the Curie−Weiss law with $g = 2.07$ and $\theta = -4.17$ K.

the diamagnetic contribution of the compound, $\chi_{diam} \approx -120 \times 10^{-6}$ emu/mol, which was estimated by using Pascal's constants. The effective magnetic moment, m_{eff}, has been calculated on the basis of the susceptibility data using the relation $m_{eff} = 2.83(\chi T)^{1/2}$. Above 50 K, m_{eff} saturates to the value of 1.78 μ_B, which is a typical value for Cu^{II} with $S = {}^1/_2$ (Figure 7, upper inset). The rapid decrease of the moment below 20 K can be ascribed to the formation of antiferromagnetic correlations in the system, which coincides with the behavior of the EPR half-width. The temperature dependence of the susceptibility obeys the Curie−Weiss law down to 10 K (Figure 7, lower inset). At lower temperatures, deviations from the Curie−Weiss law appear, and they are indicated by the presence of a round maximum observed at 3.0 ± 0.1 K (see Figure 7). Fitting the data in the temperature interval from 10 to 300 K yielded $g = 2.07 \pm 0.05$ and the Curie temperature $\theta = -4.17 \pm 0.05$ K. The negative sign of θ coincides with the behavior of the effective magnetic moment. Consequently, $zJ/k_B = -16.7$ K, where z represents the number of nearest neighbors and J stands for the exchange interaction related to the Hamiltonian

$$H = -J\sum_{i,j} S_i S_j + \sum_i g\mu_B B S_i \qquad (4)$$

To clarify the role of individual exchange paths, the low-temperature susceptibility data below 10 K characterized by

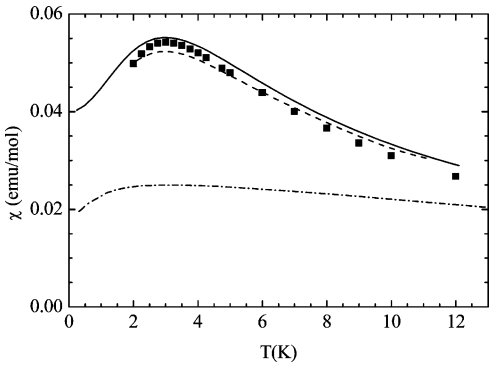

Figure 8. Temperature dependence of the magnetic susceptibility of powdered CTCL. The solid line represents the theoretical prediction for the $S = {}^1/_2$ Heisenberg chain limit ($J_1 = 0$; $J_1'/k_B = -4.5$ K), the dashed line corresponds to the square-lattice model ($J_1/k_B = -3.0$ K; $J_1' = 0$), and the dash-dotted line represents the behavior of the triangular lattice with $J_1/k_B = J_1'/k_B = -6.0$ K. All calculations are performed for $g = 2.12$.

a round maximum have been analyzed in the frame of the antiferromagnetic J_1-J_1' model with $S = {}^1/_2$. Recently, theoretical susceptibility predictions for the arbitrary J_1'/J_1 ratio have been calculated using high-temperature series expansion.[25] The theoretical studies predicted that the susceptibility for the antiferromagnetic exchange coupling shows a broad maximum at a temperature on the order of the Curie temperature. If the exchange constants are scaled to give the same peak position, the magnitude of the peak varies with frustration. The unfrustrated models represented by the square-lattice ($J_1' = 0$) and linear-chain ($J_1 = 0$) limits have similar peak susceptibilities, while the triangular lattice ($J_1 = J_1'$) deviates the most from them, having a much smaller peak value and much flatter temperature dependence. Analysis of the CTCL susceptibility within these limiting models, previously solved in ref 26, revealed rather good agreement with the predictions for the chain and square-lattice models (Figure 8) when $g = 2.12$, the averaged value calculated from the EPR experiment. The magnitude of the peak is extremely sensitive to the values of the g factor and the exchange coupling J derived from the experimental peak position that is determined with a large uncertainty. Thus, additional refinement of the J_1'/J_1 ratio will not lead to the unambiguous decision of whether the system possesses a square lattice or chainlike features. However, it is clear that the strengths of J_1 and J_1' interactions are not comparable. From the known crystal structure of CTCL, we can assume that the nearest-neighbor exchange coupling J_1 is mediated via the multiple $Cu(d_{x^2-y^2})-N-H\cdots Cl-Cu(d_{x^2-y^2})$ interactions and the next-nearest-neighbor exchange coupling J_1' is mediated via the multiple $Cu(d_{x^2-y^2})-Cl\cdots H-N-H\cdots Cl-Cu(d_{x^2-y^2})$ interactions. In this case, the J_1'/J_1 ratio should be smaller than 1, and consequently, the CTCL system might possess square-lattice-like features.[20] The value of the ratio with respect to 1 should not be changed if the Cl bridges are taken into account because the double-diagonal interac-

(25) Zheng, W.; Singh, R. R. O.; McKenzie, R. H.; Coldea, R. *Phys. Rev.* **2005**, *B71*, 134422.
(26) (a) Bonner, J. C.; Fischer, M. E. *Phys. Rev.* **1964**, *135*, A640. (b) Algra, H. A.; de Jongh, J. J.; Carlin, R. L. *Physica* **1978**, *B93*, 24. (c) Elstner, N.; Singh, R. E. P.; Young, A. P. *Phys. Rev. Lett.* **1993**, *71*, 1629.

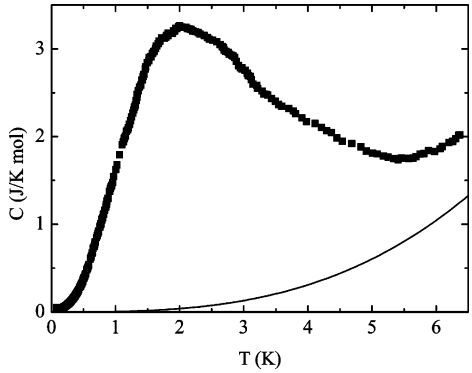

Figure 9. Temperature dependence of the total specific heat of powdered CTCL. The solid line represents a phonon contribution, C_{ph}, in the Debye approximation.

tion $Cu(d_{x^2-y^2})-Cl-Cu(d_{z^2})$ should be more efficient than $Cu(d_{z^2})-Cl-Cu(d_{z^2})$ because of crystal field effects.[27] The square-lattice behavior is also suggested by the analysis of the magnetization data (Figure 5, inset). The magnetic field dependence of magnetization has been studied at $T = 2$ K up to 50 kG. The data are clearly inconsistent with ideal, free-spin behavior that is modeled by the Brillouin function

$$M = Ng\mu_B \tanh(g\mu_B B/2k_B T) \qquad (5)$$

with $g = 2.12$ and $S = {}^1/_2$, indicating the presence of relatively strong antiferromagnetic interactions. Taking into account that the analysis of low-temperature susceptibility data yielded the best results for chain and square-lattice models, the obtained exchange constants $J_1'/k_B = -4.5$ K and $J_1/k_B = -3.0$ K, respectively, have been used for the corresponding numerical calculations of the magnetization.[28] As can be seen from the inset of Figure 5, none of the models describes the data quantitatively; however, the curvature of the experimental data seems to be better described by the square-lattice model. Using the aforementioned physical parameters and the mean-field approximation of the saturated magnetic fields, $B_{sat} = zJ/g\mu_B$, the values of $B_{sat} = 63$ and 84 kG were obtained for chain and square-lattice models, respectively. Despite the fact that the calculated M vs B dependences are valid in the ground state, i.e., $T = 0$, they reflect general features of the experimental curve, namely, the convex curvature and unsaturated magnetization values at 50 kG, albeit at finite low temperatures.

Unlike susceptibility and magnetization quantities, the specific heat of low-dimensional magnets represents a quantity with a maximum height independent of J values; the height is determined only by the corresponding model, while the position is scaled by J values. The temperature dependence of the specific heat was measured to verify the assumptions about the square-lattice character of the magnetic subsystem. The measurements were done in zero magnetic field in the temperature range from 60 mK to 6.5 K (Figure 9). The specific heat behavior is dominated by a round maximum at 2.00 ± 0.05 K without any phase transition to the ordered state down to 60 mK. The shape of the maximum suggests the presence of short-range correlations in the $S = {}^1/_2$ system. Because the compound represents a magnetic insulator, the increasing specific heat above 4 K can be ascribed to the phonon contribution. Consequently, the total specific heat, C, is determined by the sum of the magnetic and phonon contributions, C_{mag} and C_{ph}, respectively. The latter has been estimated using a standard procedure based on a finding of a temperature interval in which $C_{mag} = a/T^2$, and C_{ph} can be described by the Debye bT^3 law. Then a linear fit of the CT^2 vs T^5 plot has been performed in the range 4.5−6.5 K, providing $a = 29.65 \pm 0.50$ (J K)/mol and $b = 0.004\,83 \pm 0.0005$ J/(K⁴ mol). After subtraction of the lattice contribution (Figure 9), the magnetic entropy, S_m, was numerically calculated in the interval from 60 mK to 6.5 K, while a simple extrapolation was employed above 6.5 K toward infinite temperatures. The calculations yielded $S_m = 5.73 \pm 0.05$ J/(K mol), which represents nearly 100% of the theoretical magnetic entropy for the $S = {}^1/_2$ system. This result indicates the excellent low dimensionality of the studied compound. The specific heat maximum was analyzed using the numerical predictions for the low-dimensional magnetic models already applied in the susceptibility analysis. As can be seen from Figure 10, the specific heat data are close to the theoretical predictions for both the linear-chain and square-lattice models. The fact that the experimental maximum height is significantly lower with respect to that of the square-lattice model indicates the importance of the diagonal interaction J_1', which cannot be neglected. Theoretical studies of the ground-state phase diagram of the J_1-J_1' model[20] revealed the persistence of Néel order and gapless excitation spectra for J_1'/J_1 from 0 to about 0.6. This fact implicates T^2 dependence of the specific heat at low temperatures $T < 0.1J_1/k_B$, as derived by Kubo for a square lattice in the spin-wave approximation.[29] The appearance of a gap in the spin excitation spectrum, associated with a potential spin liquid state assumed for $J_1'/J_1 \approx 0.6-0.9$, leads to the exponential decay of the specific heat at low temperatures. The plot of experimental data in properly

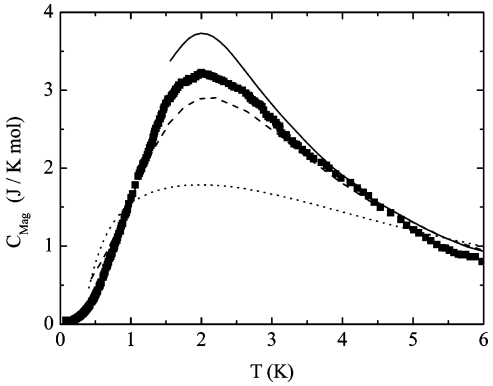

Figure 10. Temperature dependence of the magnetic specific heat of powdered CTCL. The solid line represents a theoretical prediction for the $S = {}^1/_2$ Heisenberg square-lattice limit ($J_1/k_B = -3.1$ K; $J_1' = 0$), the dashed line corresponds to the behavior of the Heisenberg chain ($J_1 = 0$; $J_1'/k_B = -4.0$ K), and the dotted line represents the theoretical prediction for the triangular lattice with $J_1/k_B = J_1'/k_B = -3.9$ K.

(27) Brown, D. B.; Donner, J. A.; Hall, J. W.; Wilson, S. R.; Wilson, R. B.; Hodgson, D. J.; Hatfield, W. E. *Inorg. Chem.* **1979**, *18*, 2635.
(28) (a) Griffiths, R. B. *Phys. Rev.* **1964**, *133*, A768. (b) Zhitomirski, M. E.; Nikuni, T. *Phys. Rev.* **1998**, *B57*, 5013.
(29) Kubo, R. *Phys. Rev.* **1952**, *87*, 568.

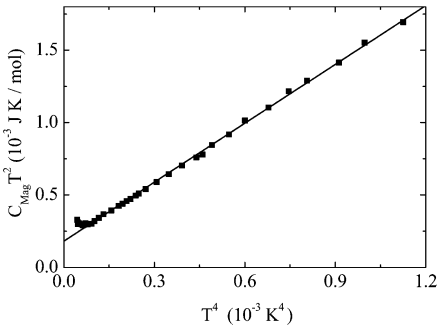

Figure 11. $C_{mag}T^2$ vs T^4. The solid line represents a linear fit with the parameters given in the text.

reduced coordinates at low temperatures excluded the exponential decrease and, correspondingly, the possibility of a gap in the excitation spectrum. Inspection of the experimental specific heat data at lowest temperatures revealed a slight increase below 90 mK. The calculations of the specific heat of nuclear Cu^{II} spins $I = {}^3/_2$ revealed that this contribution represents at the lowest temperatures only about 1% of the observed specific heat. This fact indicates that the mentioned increase can be associated with the formation of interlayer magnetic correlations as a result of dipolar interactions, leading to the onset of long-range order at temperatures significantly lower than 60 mK, the lowest achievable temperature during the experiment. Assuming that the low-temperature specific heat can be described by the sum of the aforementioned Kubo's a_1T^2 formula and the a_2/T^2 "tail" from the specific heat of a potential low-temperature λ-like anomaly, a $C_{mag}T^2$ vs T^4 plot yielded a linear dependence in the temperature range from 90 to 180 mK, which is a range of sufficiently low temperatures for the validity of the assumption (Figure 11). The fitting procedure yielded $a_1 = 1.35 \pm 0.05$ J/(K^3 mol) and $a_2 = (1.8 \pm 0.5) \times 10^{-4}$ (J K)/mol. Using De Klerk's relation for a Heisenberg magnet,[30] $a_2 = 3\Theta^2/2z$, where Θ is the Curie temperature, z is the number of nearest neighbors from adjacent layers, the interlayer coupling, J', has been estimated, and $|J'/k_B| = 3.3$ mK when assuming $z = 12$. This value coincides with nearest-neighbor dipolar coupling calculations $E/k_B \approx 2g^2\mu_B^2S^2/d^3k_B$, where d stands for an effective interionic distance between Cu^{II} ions along the a axis, being equal to $d \approx 9.5$ Å. The calculations yielded the energy of the dipolar coupling $E/k_B \approx 1.6$ mK. The obtained agreement supports our assumptions about the origin of the low-temperature specific heat increase. Using Kubo's formula, the intralayer coupling $|J_1/k_B| = 2.7 \pm 0.1$ K has been calculated from the coefficient a_1. The estimate is in good agreement with the value $J_1/k_B = -3.1$ K obtained from the application of the square-lattice model in the analysis of a round specific heat maximum. Considering the estimated values of intralayer and interlayer exchange coupling, the ratio $J'/J_1 \approx 10^{-3}$ can be obtained.

(30) De Klerk, D. *Physica* **1946**, *12*, 513.

The observed T^2 dependence of a low-temperature specific heat is a further indication of the existence of the Néel phase in the ground-state limiting the ratio J_1'/J_1 from 0 to about 0.6. Further refinement of the J_1'/J_1 ratio requires theoretical predictions for specific heat similar to the case of susceptibility, but the required expressions have not yet been derived.

Conclusions

The compound CTCL contains the [Cu($-\mu_3$-Cl$-$)Cu_2] motif, leading to the formation of a ladderlike structure composed of chains running along the crystallographic c axis. The copper atoms are hexacoordinated in a 4 + 2 form exhibiting typical Jahn$-$Teller deformation. Consistent with this deformed hexacoordination, the diffuse-reflectance UV$-$vis spectra show the respective LMCT and d$-$d transitions to the $d_{x^2-y^2}$ orbital. The X-ray structure and EPR studies revealed that the local Cu^{II} surroundings stabilize the d_{z^2} electronic ground state of the Cu^{II} ion and, consequently, enable the propagation of the exchange paths in the equatorial plane. These exchange paths can be formed mainly by intraladder and interladder hydrogen bonds connecting Cu^{II} ions into a 2D spatially anisotropic triangular lattice described by the J_1-J_1' model, with $J_1/k_B \approx -3$ K and $J_1'/J_1 = 0-0.6$. The weak interlayer exchange coupling, $J' \approx 10^{-3}J_1$, shows that CTCL is an excellent example of a low-dimensional magnetic system useful for studies of various physical phenomena in a wide range of temperatures and magnetic fields.

We hope that quantum-mechanical calculations that will be performed soon may enlighten the role of hydrogen bonds in the magnetic properties of CTCL. Alternatively, we plan to tune the magnetic properties of the structure by a partial deuteration in order to disturb the hydrogen-bonding system and correspondingly to weaken or eliminate some magnetic interactions. The modification of the structure can be achieved by ligand substitution, magnetic dilution, and application of pressure. Because the energy of the hydrogen bonds is much lower than that of the covalent ones, it can be expected that the latter procedure should predominantly influence the system of hydrogen bonds, i.e., the symmetry of a magnetic lattice.

Acknowledgment. We are grateful P. Skyba for helpful discussion about nuclear specific heat. This work was supported, in part, by the Slovak Grant Agency VEGA (Grants 1/0447/03 and 1/0430/03), Grant APVT/20005204, and the National Science Foundation (Grant DMR-0305371). Material support from U.S. Steel DZ Energetika is gratefully acknowledged.

Supporting Information Available: X-ray crystallographic file, in CIF format, for the structural determination of the title compound. This material is available free of charge via the Internet at http://pubs.acs.org.

IC0516109